18

Microstructural Evolution in α-Al_2O_3 Compacts During Laser Irradiation

Marina Vlasova, Mykola Kakazey and
Pedro Antonio Márquez -Aguilar
CIICAp-Universidad Autonoma del Estado de Morelos,
Cuernavaca, Morelos
Mexico

1. Introduction

Laser opening (Ali et al.,1960; Maiman, 1960 ; Townes, 1960) and development of many various types of lasers (Goodison, 2008; Injeyan & Goodno, 2011; Träger, 2007; Weber, 2001) stimulated their wide practical application (Rastogi & Asundi, 2011; Ready, 2001; Ready, 1971; Webb & Jones, 2003; Weber, 1994). The basic properties distinguishing laser radiation from radiation of usual light sources are intensity, an orientation, monochromaticity and coherence (Ready, 1971). The important role has both maximum peak pulse power, and possibility to allocate energy in the set point of space. More important characteristic, than the absolute value of peak power, is a power on an unit of surface of target. The directivity, monochromaticity and coherence of laser beam allow to focus laser light into a spot of very small size. Depending on intensity and duration of action of laser radiation, the following stages of interaction of radiation with a treated material distinguish: supply of laser radiation to a material, an absorption of a light flux and transfer of its energy to a solid body, heating of a material without visible destruction, a melting of material, evaporation and elimination (ablation) of products of destruction, electronic and ionic emission from the surface, plasma formation, cooling of a material after the ending of laser influence (Shishkovskii, 2009). Selective laser sintering (SLS) of powders is one of new technologies of obtaining of superficial coverings from nano-structured materials (Deckard, 1988). This direction results to develop a concept model of prototypes ("Rapid Prototyping"). This is method of formation of 3d-model level-by-level sintering of powder materials (Gebhardt & Hancer, 2003). At first, main direction of works of SLS had practice character: an obtaining of a material with specified properties, and with specified forms, etc. At the same time, the high-speed heating inherent to laser influence in processes of SLS and the technologies integrated with it, opens possibilities for investigation of features of diffusion, kinetic, structurally-phase, rheological, and mechanical processes, in conditions far from equilibrium and poorly studied. In the present work we will bring some results of investigation of the reactionary and structural changes proceeding in pressings from mixtures of α-Al_2O_3 and α-Cr_2O_3 powders at their superficial laser treatment. An important moment here is that the processed system (pressings) also is under nonequilibrium condition.

Alumina (α-Al_2O_3) has many industrial applications, including refractory bricks, electric insulators, and protective coatings (Dorre & Hubner, 1984; Gebhardt & Hancer, 2003). So alumina ceramics is used in nuclear power plants as a heat and an electric insulator in the active zone, for IR windows or as armor for low threat applications where thinner tiles can be used (Pampuch & Haberko, 1997; Shevchenko & Barinov, 1993; Tretyakov, 1987; Wefers & Misra, 1987). Its properties can be changed significantly by the introduction of different impurity centers. Among corundum-based ceramics, ruby, which is a solid solution of chromium ions in the solid structure of covalent Al_2O_3, is the most extensively used material. Ruby single crystals are used as working elements of lasers. The compounds α-Al_2O_3 and α-Cr_2O_3 are isomorphous and their mutual solid solutions α-$Cr_xAl_{2-x}O_3$ form a single phase with a corundum structure within the composition range $0 \le x \le 2$. The method of horizontal directed crystallization (HDC) is widely used in the synthesis of large corundum (sapphire) and ruby monocrystals (Bagdasarov, 2004; Bagdasarov & Goryainov, 2001; Bagdasarov & Goryainov, 2007; Lukanina et al., 2006; Hurle,1994; Lyubo, 1975). The HDS method consists in the following (Bagdasarov, 2004): a mixture in the form of a powder, crystal breakage, or ceramic tablets is loaded into a boat-shaped container. By moving this container through the heating zone, the mixture is melted, and then the melt is crystallized in the cold zone. To obtain a strictly oriented monocrystals, a seeding agent is placed in the top of boat, after which both the moment of crystallization and the shape of the crystallization front in the process of monocrystal growth is monitored. The thermophysical processes play a decisive role in the crystallization of high-quality monocrystals because they are responsible for the generation of substantial internal mechanical stresses, porosity, and high dislocation density (Bagdasarov & Goryainov, 2001; Bagdasarov & Goryainov, 2007; Denisov et al., 2007; ; Dobrovinskaya et al., 2009; Lukanina et al., 2006; Malukov et al., 2008).

In recent years, along with traditional powder metallurgy methods for the synthesis of corundum ceramics, SLS has been used (Liu et al., 2007; Shishkovskii, 2009; Shishkovsky et al., 2007; Subramanian & Marcus, 1995; Subramanian et al., 1993; Xu et al., 2005), what makes it possible to combine complete and partial melting in a single cycle. The next stage of development of this technology is layer-by-layer SLS.

Results of investigations of the laser melted specimens (Ferkel et al., 1997; Majumdar et al., 2004; Triantafyllidis et al., 2002; Triantafyllidis et al., 2004; Wang et al., 2004; Zum-Gahr et al., 1995) show that laser scanning influences significantly the surface morphology, microstructure, and phase components of laser-treated zones. Thus, the laser treatment of the surfaces of ceramic samples, accompanied by its melting and resolidification, can be successfully used to modify their surface properties. In this the processes proceeding during laser treatment of powder mixtures of different compositions deserve particular attention. So, the temperature conditions, fast melting - fast crystallization, produced during the process is an interesting direction of preparing new ceramic materials (on the basis of mixes of powders with various temperature properties) in which a controlled inhomogeneous distribution of the impurities, the phases, etc. can be realized. In layer by layer SLS of corundum, additives which play the role of binders of grains of the basic material in the stage of powder pressing and sintering are introduced in Al_2O_3 powder to provide the required density and strength of the consolidated material (Bai & Li Y. 2009; Ferkel et al., 1997; Shishkovskii, 2005; Shishkovsky et al., 2007; Subramanian & Marcus, 1995; Subramanian et al., 1993). Among these methods are SLS of both α-Al_2O_3 (Da Shen et al., 2007; Zhao et al., 2003) and α-Al_2O_3-α-Cr_2O_3 (Nubling & Harrington, 1997; Quispe Cancapa et al., 2002; Yen, 1999).

A large number of studies by different methods were performed on dilute both low-chromium and high-chromium α-Al_2O_3 solid solutions (Carman & Kroenke 1968; de Biasi & Rodrigues 1985; Galoisy & Calas 1993; Manenkov & Prokhorov, 1955; O'Reilly & Maciver, 1962; Statz et al., 1961; Stone & Vickerman 1971;). Gradual increases in the *a* and *c* parameters of the hexagonal unit cell of the corundum structure with increasing chromium concentration were noted (de Biasi & Rodrigues 1985). The fine structure of the electron paramagnetic resonance (EPR) spectrum of the ion Cr^{3+} in corundum crystal was investigated (Manenkov & Prokhorov 1955). Four types of EPR spectra were observed in α-$Cr_xAl_{2-x}O_3$ polycrystalline specimens (Carman & Kroenke, 1968; Stone & Vickerman 1971).
This work is concerned with an experimental investigation of the surface solutionizing, crystallization, microstructure, and properties induced by a laser beam in pressings of α-Al_2O_3 + *n*α-Cr_2O_3 powders with using EPR spectroscopy, X-ray diffraction and electron microscopy methods. In the methodical plan the work is constructed in the following way. In the beginning of the work we will consider evolutionary processes in compacted α-Al_2O_3 + α-Cr_2O_3 mixtures at one-pass laser treatment. Farther we will examine the layer by layer laser sintering of Al_2O_3-xCr_2O_3 powder mixture. After that the laser surface solutionizing and crystallization in Al_2O_3-xCr_2O_3 pellets will be analyzed. And then will be discussed the laser synthesis of crystalline ruby rods from Al_2O_3- xCr_2O_3 ceramic rods.

2. Experimental procedure

2.1 Initial reactives

Commercially available α-Al_2O_3 and α-Cr_2O_3 (Reasol, Reactivo Analitico) with a particle size of 40 nm and 1.8 nm, respectively, were used as starting materials. Powder mixtures of α-Al_2O_3 + *n*α-Cr_2O_3 with *n* = 0.1 wt %, 0.5 wt %, 1.0 wt %, 3.0 wt %, 5.0 wt % and 10.0 wt % were homogenized mixing in ball mill with a low rotation rate (around 50 rpm) during 30 min.

2.2 Preparation of samples for laser processing

On the base of these powder mixtures a series of cylindrical specimens (pellets and cores) with a diameter 3 – 30 mm and a thick (length) of 3 to 15 mm were made by axial pressure, *P* (to 5 MPa) or isostatical pressure (to 5 GPa). Also was using the extrusion technology for obtaining of cylindrical specimens with a diameter 3 mm and a length of 10 to 15 mm with their subsequent sintering at 1200 ^oC.

2.3 Laser processing

The laser processing of the samples was carried out with using a 10.6 μm CO_2 laser (CW-CO_2 Spectra Physics 820, the output power was 130 W) and LTN-103 continuous-action Nd^{3+}:YAG laser (λ = 1064 nm, maximum output power is ~ 200 W, Russia). Different conditions of irradiation: the diameter of the laser spot (d), the scanning velocity (v), the irradiation power (P) were used.
In case of trying out an experiment on horizontal directed crystallization (HDC) of ruby the LTN-103 laser, d = 0.2 mm and d = 0.8 mm, v ~ 0.0094 mm/s 0.019, and 0.075 mm/s, P ~ 70 W were used. The laser irradiation was performed along long axes of the compacts prepared by using extrusion technology and following thermal treatment at 1200 ^oC for 1 h. The compacts have a diameter 3 mm and a length of 10 to 15 mm. Specimens were placed in channels formed on surfaces of compacts made from the same mixture by one-pass treatment with a laser beam. After irradiation, the specimens had the shape of rods with a length of 5 to10 mm and a diameter of 1.5 to 2 mm.

In more details conditions of laser treatment of specimens are given in the beginning of paragraphs 3.1, 3.2, 3.3 i 3.4.

2.4 Experimental methods

The initial samples and the laser-treated (LT) sample surface were characterized using powder XRD (Siemens D-500) in CuK_α radiation.

The method of Electron Paramagnetic Resonance (EPR; SE/X 2547-Radiopan; x-ray range; at room temperature) spectroscopy was used to study the different paramagnetic centers (PC) in LT-samples. EPR-recording was carried out through the whole volume of specimens. EPR-measurements were also performed depending on the angle between the external magnetic field and an LT-surface of a specimen. Also, single crystal of Cr doped α- Al_2O_3 was used in this studies.

Infra Red (IR) spectra were obtained with a Specord M80 spectrometer (Karl Zeiss, Germany).

An electron microscopy study was performed with a Superprobe-733 scanning electron microscope (JEOL, Japan) and a SEM/FIB NOVA 200 system (Bruker, Gemany).

3. Experimental results and discussion

3.1 One-pass laser treatment of powder pellets of Al_2O_3- xCr_2O_3

Using the laser facility, one-pass treatment of the surface of a pellets prepared at 5 MPa were performed at P = 60, 70, 160 and 190 W. The scanning velocity (v) of laser beam was 0.075, 0.15, 0.25, and 0.3 mm/s. The size of laser beam was d = 0.2 – 0.6 mm. In this case, concave channels formed on the surface (Fig. 1a). On the surface, one can see arcs. Theirs formation is a result of melting → cooling of corundum during transverse of the laser beam. On the lateral walls of the channel, strips formed as a result of dissociation of Al_2O_3 (Fig. 1 b) are seen. The depth of the channel, the thickness of the melting-recrystallized layer (h_1), and zone of sintering (h_2) depends on irradiation parameters, namely, the irradiation power and the traverse speed of the laser beam (Fig. 2) (Vlasova et al., in pres. accept.). In Fig. 3, the growth of corundum crystallites from the bottom part of the track to its surface is shown. The color of the superficial layer changes from pink to deep-brown depending on the α-Cr_2O_3 amount in the initial specimen. Also the color changes from superficial to a zone of sintering and further up to initial colour of compacted mixture.

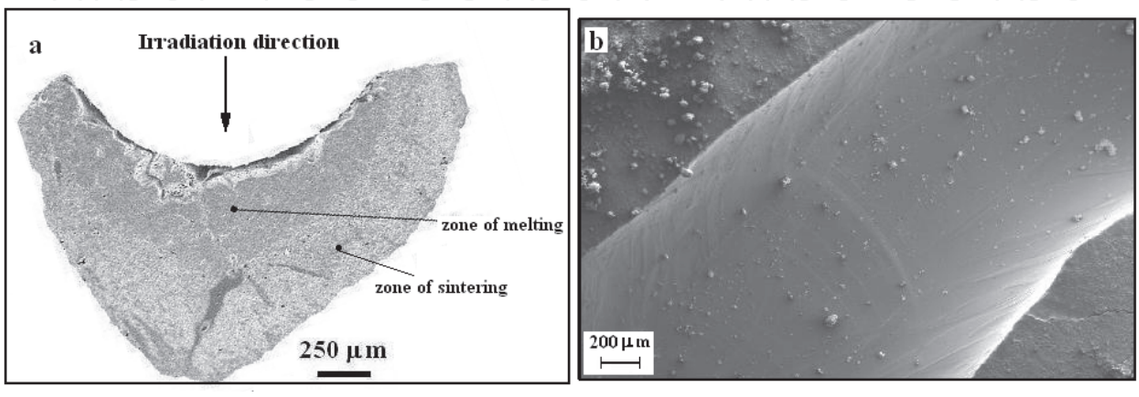

Fig. 1. Micrographs of channels formed in one-pass laser treatment of a compact at P = 160 W and v = 1.25 mm/s. (a) cross section; (b) the top view.

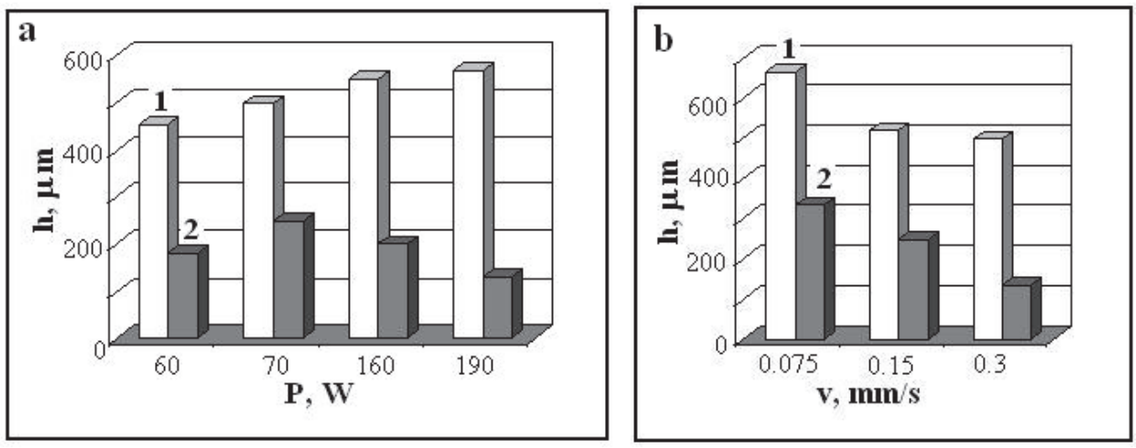

Fig. 2. Changes in the maximal thicknesses of the recrystallized layer (1) and sintered layer (2) depending on the power (a) and the traverse speed (b) of the laser beam in one-pass laser treatment. For (a) at v = 0.15 mm/s. For (b) P = 70 W.

IR absorption spectra of corundum for different layers of the material located under the track illustrate the gradual weakening of the band at v_2 ~ 500 cm^{-1} as the distance to the track decreases (Fig. 4, spectra 2–6). The weak intensity of band v_2 is characteristic for a ruby. A spectrum obtained from the track is assigned to the IR spectrum of α-Al_2O_3 (Vlasova et al., 1972) (see Fig. 4, spectra 1, 2 and 6). For the superficial layer of track, the intensity of the spectrum appears to be much weaker than for the subsurface layers. The weakening (see Fig. 4 curve 1) is connected with the gradual defects accumulation and increasing electroconductivity in the surface layer of the track.

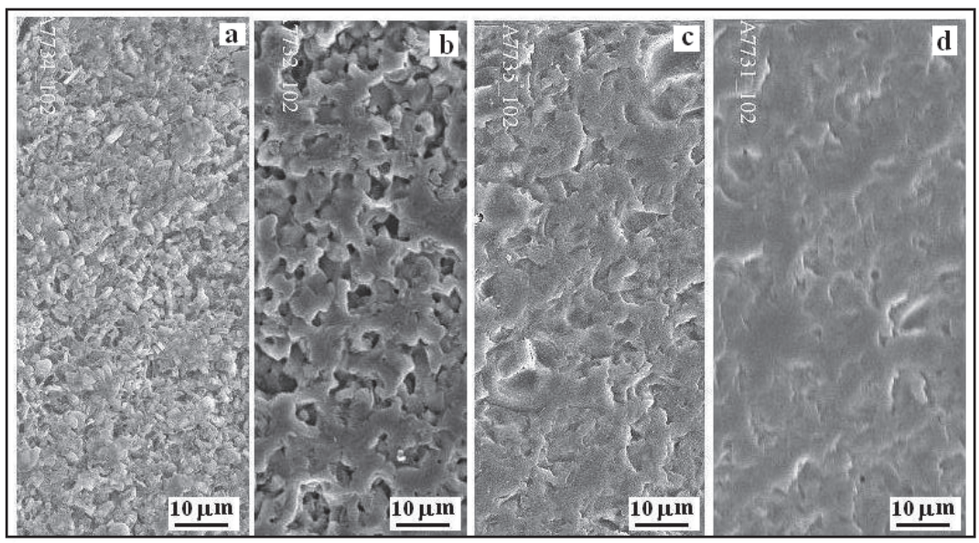

Fig. 3. Micrographs of channels formed in one-pass treatment at P = 70 W and v = 0.075 mm/s: (a)–(d) correspond to the direction of photographing from the bottom of the channel to its surface.

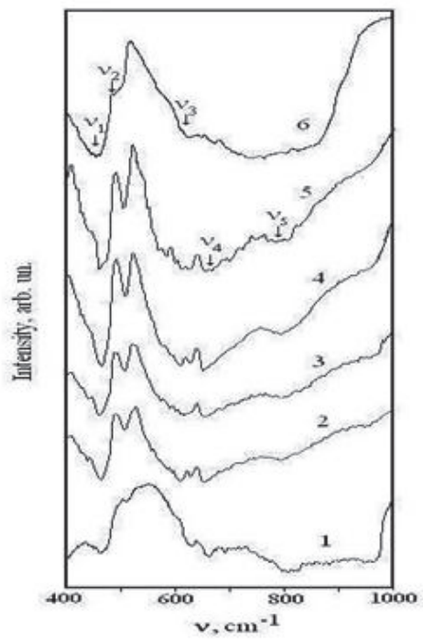

Fig. 4. IR absorption spectra of the superficial layer of a track (1) and in layers under the superficial layer by 0.5 μm (2), 1.0 μm (3) and 1.5 μm (4). Comparison of spectra of corundum (5) and ruby (6). The sample:KBr ratio is 1:150 for spectrum (1) and 1:300 for spectra (2-6).

3.2 Layer by layer laser treatment of pellets of Al_2O_3- xCr_2O_3 (Vlasova et al., 2010)

An experiments on the layer-by-layer selective laser sintering (SLS) were carried out on pellets obtained by axial pressing at P = 5 MPa. Used capacities of the LTN-103 laser were P ~ 90, 120, 160, and 190 W, v ~ 0.13 mm/s 0.13, 0.26, 0.4, 0.64, and 1.25 mm/s, d = 0.2 mm. The system of vertical movement of a sample without changes in the size of the laser spot enabled us to perform additional operations on the surface of compacts. At the beginning the unitary treatment of surface of compact by laser beam was carried out. At multiple-run treatment an originally formed concave track was filled up by the powder mixture. A powder was consolidated and planed. After this procedure a filled channel was subjected to irradiation. The procedure of filling of the channel by a powder mixture and its irradiations again was repeated. The number of such backfills of channel and procedure of irradiation was from 2 to 12. Gradually above the specimen surface a convex track appeared. The height of backfill inside each series of experiments was constant. A series of experiments was realized in which the height of backfills was different: h_1 = 125 μm, h_2 = 250 μm, h_3 = 350 μm, and h_4 = 500 μm.

As the layers build up, the thickness of the new-formed product (α-Al_2O_3) gradually increases (Fig. 5). This means that, in the chosen mode of treatment, not the whole volume of the backfill is melted and recrystallized. Most pores and cracks are present between the layers. The size and the number of pores increase as the traverse speed of the laser beam rises. These data show that to obtain a low-porosity track material, it is necessary to reduce substantially the traverse speed of the laser beam. As a result, a new-formed liquid phase can fill cavities, pores, and cracks of the underlying layer. Note that, as a result of the

dissociation and ablation of Al_2O_3 (Vlasova et al., 2010) the largest number of cavities and channels form in the surface layers of tracks. As in a case of the one-layer tracks, with decrease in v at a rather low power (P ~ 60–70 W), the thicknesses of the layers h_1 and h_2 increase. At a low traverse speed of the laser beam, a multilayered building-up of corundum (layer h_1) is accompanied by a decrease in the thickness of the sintered layer (h_2). It is likely that cause of this effect is the high thermal conductivity of corundum.

X-Ray measurements and EPR investigation of spectrum of Cr^{3+} in polycrystalline Al_2O_3 haven't revealed appreciable differences in different layers.

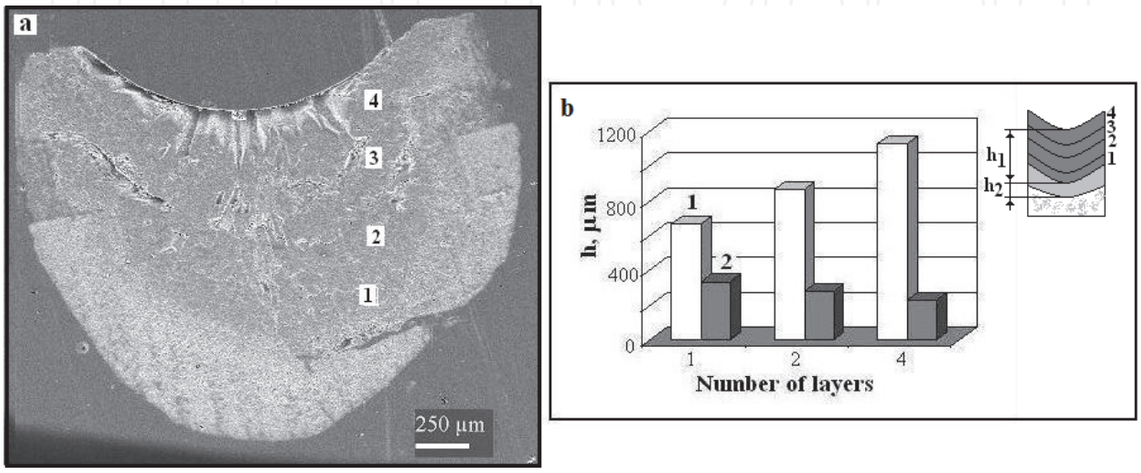

Fig. 5. Micrographs of channels formed in four-run treatment (a) and changes in the maximal thicknesses of the recrystallized layer (1) and sintered layer (2) depending on the number of backfills at (b). P = 70 W, v = 0.075 mm/s. 1–4 correspond to the numbers of layers.

3.3 Laser surface treatment of powder pellets of Al_2O_3- xCr_2O_3 (Kakazey et al., 2009)

For irradiation of pellets obtained by hydrostatic pressure at 5 GPa, the CO_2-laser with P = 130 W, d = 0.3 mm, v = 0.7 mm/s were used. Three laser scannings of the same trace were performed in a spiral motion with a step of 0.25 mm beginning from the center of a pellet.

During one-pass laser treatment of dense pellets, concave tracks also forms on their surfaces. However, in this case, the depth of tracks is much smaller than that in the case irradiation of loose powder specimens. The thickness (h_1) of the formed ruby layer is ~0.3 mm even under high-power irradiation (160–190 W). The thickness of the sintering zone is comparable or slightly larger than the thickness of the recrystallization zone. On a chip of a track (Fig. 6), we can see that a sintering zone transforms into a recrystallization zone and that corundum crystallites increase in size as the distance to the surface of the track decreases. On the surface of the track, cracks, boundaries of crystallites, and striation, which appears due to the ablation of the track material, are present. So, the growth of crystallites occurs from the lower layers of pellets to the surface. Crystallites are initially directed perpendicularly to the surface of the track. However, as the distance to the surface decreases, crystallites begin to deviate from vertical to horizontal direction. They take the bent shape and an identical orientation, i.e., texturing that is set by the traverse of the laser beam occurs.

For the given case it was possible to carry out the x-ray analysis of the irradiated tracks without destroying specimen. The XRD pattern of the initial sample is shown in Fig. 7 (1).

The positions and normalized intensities of their X-ray peaks are very close to those of X-ray peaks for an ideal powder specimen consisting of the α-Al_2O_3 and α-Cr_2O_3 (JCPDS-International Centre for Diffraction Data, 1999) (see Table 1). The XRD patterns of superficial layer of different LP-samples (with different contents α-Cr_2O_3) are shown in Fig. 7 (2-6). The normalized intensities of the LT samples (see Fig. 7 and Table 1) show the presence of the following preferred orientations of α-Al_2O_3 crystallites: [1010] in an α-Al_2O_3 + 0.1% α-Cr_2O_3 sample; [116] in an α-Al_2O_3 + 0.5% α-Cr_2O_3 sample; [116] and [113] in an α-Al_2O_3 + 1.0% α-Cr_2O_3 sample; [116] in an α-Al_2O_3 + 5.0% α-Cr_2O_3 sample; [116] and [012] in an α-Al_2O_3 + 10.0% α-Cr_2O_3 sample. The normalized intensities of α-Cr_2O_3 in LT α-Al_2O_3 + 10.0% α-Cr_2O_3 sample show (Fig. 7) that the [110]-preferred orientation of α-Cr_2O_3 crystallites take place.

2-Theta	(h k l)	d(nm)	I_{theor}	I_{exp} Init. 10.0%	I_{exp} LT 0.1%	I_{exp} LT 0.5%	I_{exp} LT 1.0%	I_{exp} LT 5.0%	I_{exp} LT 10.0%
25.568	(0 1 2)	0.3479	683	370	20			130	999
35.140	(1 0 4)	0.2552	999	840	< 10		250		65
37.763	(1 1 0)	0.2379	460	370	< 10		220		250
43.339	(1 1 3)	0.2085	961	999	40		550		220
46.183	(2 0 2)	0.1964	2.0	3.0	60			130	
52.533	(0 2 4)	0.1740	467	470	10			270	
57.482	(1 1 6)	0.1601	906	940	100	999	999	999	900
66.493	(2 1 4)	0.1404	343	340	85		50		
68.181	(3 0 0)	0.1374	521	550			340		
76.854	(1010)	0.1239	145	180	999				

Table 1. Diffraction data for α-Al_2O_3.

In the initial α-Al_2O_3 + *n*α-Cr_2O_3 samples, only a weak broad EPR signal, which was due to defect states of the α-Cr_2O_3 phase, was registered at $g \sim 1.9$. In Fig. 8, the room-temperature EPR spectra of laser-treated α-Al_2O_3 + *n*α-Cr_2O_3 samples are shown. Some singularities (I—IV at $g_I \approx 1.22$, $g_{II} \approx 1.47$, $g_{III} \approx 3.38$, and $g_{IV} \approx 22$) of different intensities and shape were found in the EPR spectra.

The EPR spectra of Cr^{3+} ions in the Al_2O_3 lattice may be described by the axial spin Hamiltonian

$$H = g\beta BS + D\left[S_z^2 - \frac{1}{2}S(S+1)\right] \tag{1}$$

with parameters g = 1.984 and D = 5.746 GHz (Manenkov & Prokhorov, 1955). In polycrystalline samples the EPR spectrum represents a set of singularities (narrow signals) which position is defined by expression

$$\left|\nabla_0 B_r(\theta,\phi)\right| = \left[\left(dB_r/d\theta\right)^2 \Delta\theta^2 + 1/\sin^2\theta \left(dB_r/d\phi\right)^2 \Delta\phi^2\right)\right]^{1/2} = 0, \tag{2}$$

where $B_r(\theta,\phi)$ is angular dependence of fine structure EPR-lines in crystal, θ and ϕ are specify the spherical coordinates giving the relative orientation between direction of magnetic field B and the crystal axes (Kliava, 1988). The EPR spectrum of Cr^{3+} (singularities I—III) in Al_2O_3 polycrystalline samples is well known (Carman & Kroenke, 1968; de Biasi & Rodrigues, 1985; O'Reilly & Maciver, 1962; Stone & Vickerman, 1971). In order to identify signal IV, we compared the EPR spectrum for polycrystalline samples with an angular dependence of EPR curves of Cr^{3+} in ruby crystals (Fig. 8). In Fig. 9, we show that singularities I, II, III, and IV correspond to the EPR transitions (Cr^{3+}:Al_2O_3) -3/2 ↔ -1/2 (θ = 90°), -1/2 ↔ +1/2 (θ =35°), +1/2 ↔ +3/2 (θ =90°) and a forbidden transition (FT) (θ = 0 – 30°), respectively.

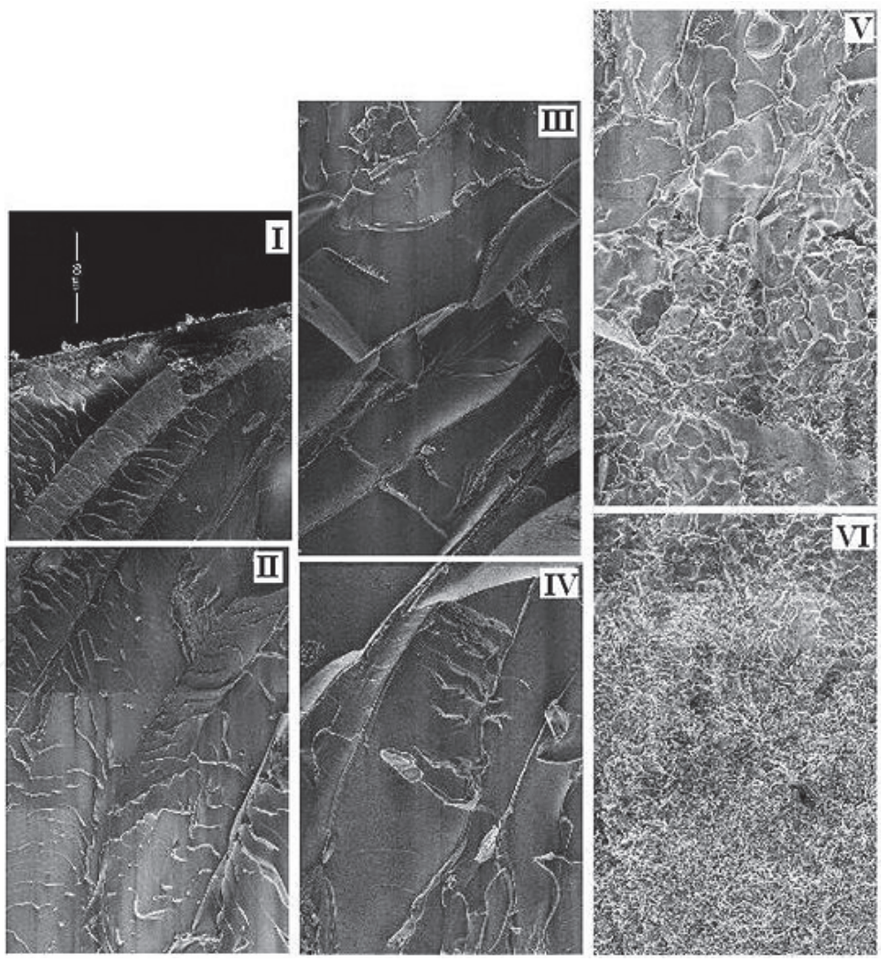

Fig. 6. Micrographs of the longitudinal section of channel. I → VI corresponds from the surface of channel to the bottom.

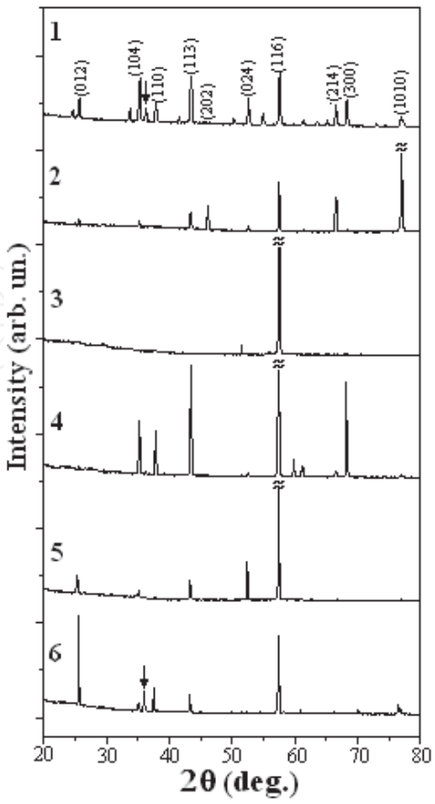

Fig. 7. X-ray diffraction patterns of α-Al_2O_3 + *n* α-Cr_2O_3 samples before and after LT: 1 , *n* = 10 wt. %, initial; 2, *n* = 0.1%, LT; 3, *n* = 0.5%, 4, *n* = 1.0%, LT; 5, *n* = 5.0%, LT; 6, *n* = 10.0%, LT. The arrow in 1 and 6 diffraction patterns indicates the (110) peak of α-Cr_2O_3.

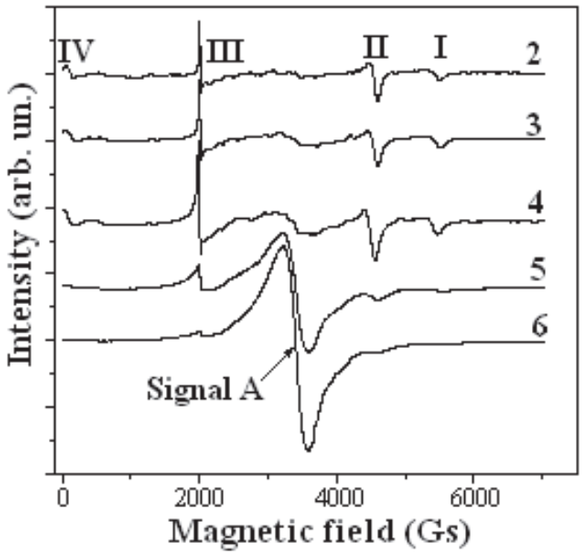

Fig. 8. EPR spectra in α-Al_2O_3 + *n*α-Cr_2O_3 laser treated samples. I - IV are designations of singularities (see text). 2, samples with *n* = 0.1% after LT; 3, *n* = 0.5%, 4, *n* = 1.0%, LT; 5, *n* = 5.0%, LT; 6, *n* = 10.0%, LT.

In Fig. 10, dependences of the amplitudes of singularities II and III on the angle φ between the external magnetic field and a perpendicular to the LT surface of a sample are presented. A decrease in the amplitude of the EPR singularity II and an increase in the amplitude of the EPR singularity III are observed as the angle φ increases from 0 to 90°. An increase in the amplitude of the EPR singularity II and a decrease in the amplitude of the EPR singularity III are observed as the angle φ increases from 90 to 180° (Fig. 10).

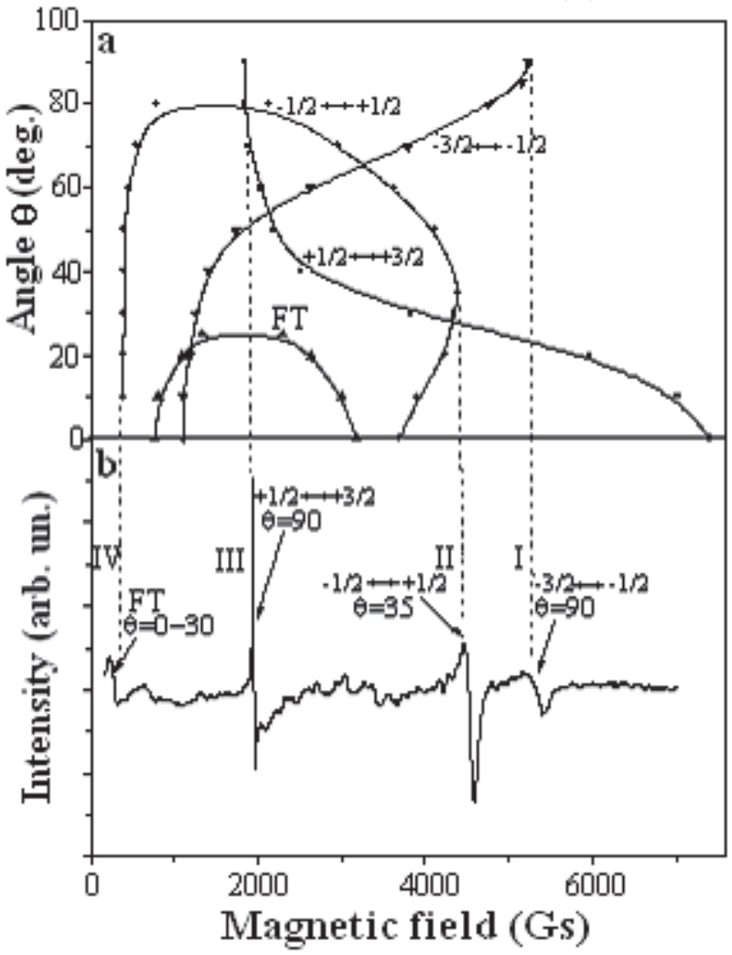

Fig. 9. The observed angular dependence of the EPR spectrum of Cr^{3+} ions in α-Al_2O_3 single crystal (a) and EPR spectrum in an α-Al_2O_3+0.1%α-Cr_2O_3 LT sample (b). I—IV are designations of singularities.

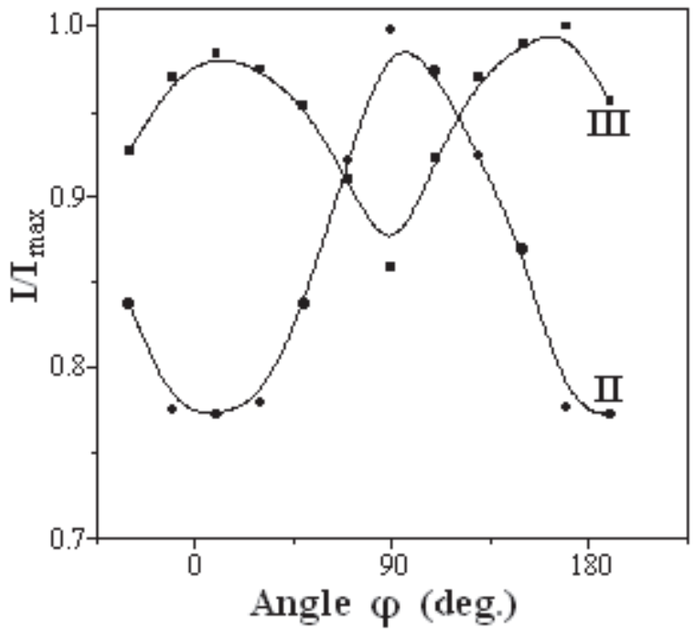

Fig. 10. Variations the I/I_{max} ratio for EPR-singularities II and III in an LT α-Al_2O_3 + 0.1% α-Cr_2O_3 specimen as functions of the angle φ between the external magnetic field and the perpendicular to the LT-sample surface.

At n > 1 wt %, in the α-Al_2O_3 + nα-Cr_2O_3 samples, decreases the amplitudes of singularities I—IV, the appearance and an increase of a new signal A at $g \approx 1.98$ are observed (Fig. 8). The decreases of the amplitudes of the singularities I—IV is accompanied by increases peak-to-peak line width and by the smearing of line. The width of signal A decreases with increasing n (ΔB_A is ~ 520 Gs for n = 1.0 wt %, ~ 380 Gs for n = 5.0 wt %, and ~ 320 Gs for n = 10.0 wt %). The A signal intensity is nearly proportional to the α-Cr_2O_3 on the amount in the initial samples.

The initial samples consist of mechanical mixtures of α-Al_2O_3 and α-Cr_2O_3 particles. The melting point of Al_2O_3 is 2046 °C and the melting point of Cr_2O_3 is 2334 °C. During high-temperature laser treatment, the fully melting of the α-Al_2O_3 particles and partially melting of the α-Cr_2O_3 particles occurs in the processed surface layer of sample (Fig. 6). The formed Al_2O_3 melt covers α-Cr_2O_3 particles. In this case, α-Cr_2O_3 particles dissolve gradually in the α-Al_2O_3 melt. However, as a result of the relatively short treatment, complete dissolution of α-Cr_2O_3 particles does not occur in the Al_2O_3 melt (Fig. 7). At cooling, the directed crystallization of the formed ceramic material takes place. In the wide class of ceramics, the orientation of crystallites is not usually distributed randomly, as in the case of an ideal powder sample. The observed differences in the preferred orientations of α-Al_2O_3 crystallites in crystallized layers of different samples indicate some unsystematic character of the preferred direction of crystallization. Though the [116] orientation, one of some preferred orientations of crystallization, take place in LT α-Al_2O_3 samples with 0.5%, 1.0%, 5.0% and 10.0% α-Cr_2O_3. In such surface layer the undissolved α-Cr_2O_3 particles also show the preferred orientation. Preferred orientations in surface crystallized layers and particles Cr_2O_3 in stiffening Al_2O_3 melt may be connected with the anisotropic shape of initial particles α-Al_2O_3 and α-Cr_2O_3.

During LT, the whole sample is subjected to the temperature influence. Parameters of the influence in different regions of the samples are determined by their geometry, thermal conductivity, etc. Dissolution of Cr_2O_3 particles in α-Al_2O_3 leads to appearance of the EPR spectra of Cr^{3+} centers in α-Al_2O_3. Let us consider the formation of EPR spectra at a spatial homogeneous concentration distribution of paramagnetic centers (PC) in samples.

3.3.1 EPR Spectra at a homogeneous distribution of impurities in samples

In general, at low impurities concentration ($c < 0.05\%$), the shape and width of an individual EPR signal are determined by relaxation parameters. In this case, I is proportional to the amount of PC in the specimen, i.e., to c. At higher concentration, dipole–dipole broadening, which is proportional to the impurity content, manifests itself (Berger et al., 1995; Kittel & Abrahams, 1953). By generalizing results of (Berger et al., 1995; Kittel & Abrahams, 1953) for $S = 3/2$, we obtain

$$\Delta B_{dd} \approx 8\beta g\left(\frac{c}{d^3}\right) \tag{3}$$

where d is the shortest distance between paramagnetic ions, c is concentration in mole percents. Note that ΔB_{dd} is about 1000 Gs at chromium concentration in the sample of 15 mol %. In complex EPR spectra different lines may have different widths ΔB_{ind}, and their changes with increasing ΔB_{dd} require individual consideration. In groups of closely located lines (GL) their overlapping occurs with increasing linewidth and a single signal (SS) forms. Note that the signal assigned to the β_1 phase in (Carman & Kroenke, 1968; Stone & Vickerman 1971) is most likely connected with the superposition of wider (than I—IV) curves in the central part of the spectrum (see spectra 3 and 4 in Fig. 8 and curves for $-1/2 \leftrightarrow +1/2$ and FT transitions in Fig. 9).
At $c > 15$ mol %, we should expect the exchange-interaction-related phenomena, which lead to the exchange narrowing of dipolar broadening (Barnes, 1974). Thus, signal A (Fig. 8) is a typical EPR signal in highly concentrated α-Al_2O_3 + nα-Cr_2O_3 samples (β_N phase (Carman & Kroenke 1968; Stone & Vickerman 1971)). It is due to the development of dipole and exchange (a mixture of ferromagnetic and antiferromagnetic) $Cr^{3+} - O - Cr^{3+}$ interactions (Stone & Vickerman 1971). And in α-Cr_2O_3, a final antiferromagnetic mechanism of exchange interaction sets up.
From the performed analysis it follows that at a homogeneous distribution of the impurity, as its content increases, the gradual transition from the spectrum of individual atoms to EPR spectra of highly concentrated states occurs. The use of formula (2) and data of experimental works (Carman & Kroenke, 1968; Knappwost & Gunsser, 1959; Poole & Itzel, 1964; Stone & Vickerman 1971; Wenzel & Kim, 1965) makes it possible to construct a rough dependences of changes in the linewidths of EPR signals in $Cr_xAl_{2-x}O_3$ samples at $0 \le x \le 2$ (Fig. 11, the solid curve for $T \sim 400$ K. For α-Cr_2O_3 the Neel temperature is 307 K (McGuire et al., 1956). The case the concentration range from 0 to ~ 3.5 wt % of Cr_2O_3 (zone A) is favorable for precise recording the EPR spectra from individual PC. The case the concentration of PC range from 3.5 wt % to 55.0 wt % (zone B) is unfavorable for precise recording EPR spectra due to large widths of signals. The case the concentration of PC range from 55.0 wt % to 100.0 wt % (zone C) is favorable for recording EPR spectra from exchange-related complexes.

3.3.2 EPR Spectra at an inhomogeneous distribution of impurities in specimens

The discrepancies between measured and calculated values for the linewidths or the simultaneous existence of two or more EPR spectra, which are characteristic for different

concentration states of impurities, indicate an inhomogeneous distribution of impurities in the samples. Thus, the recording of two distinctly different EPR spectra, namely, from individual Cr^{3+} ions (signals I - IV) and the signal from highly concentrated states of $Al_{2-x}Cr_xO_3$ (signal *A*) (Fig. 8) shows the high degree of inhomogeneity of distribution of the chromium in our samples. Note that, in most works on the EPR investigation of the α-Al_2O_3 + $n\alpha$-Cr_2O_3 samples with even a small value of *n*, a similar situation can be observed (Carman & Kroenke, 1968; O'Reilly & Maciver, 1962). This indicates that the preparation of α-$Al_{2-x}Cr_xO_3$ samples with a homogeneous distribution of chromium impurities by solid-state synthesis is an intricate problem.

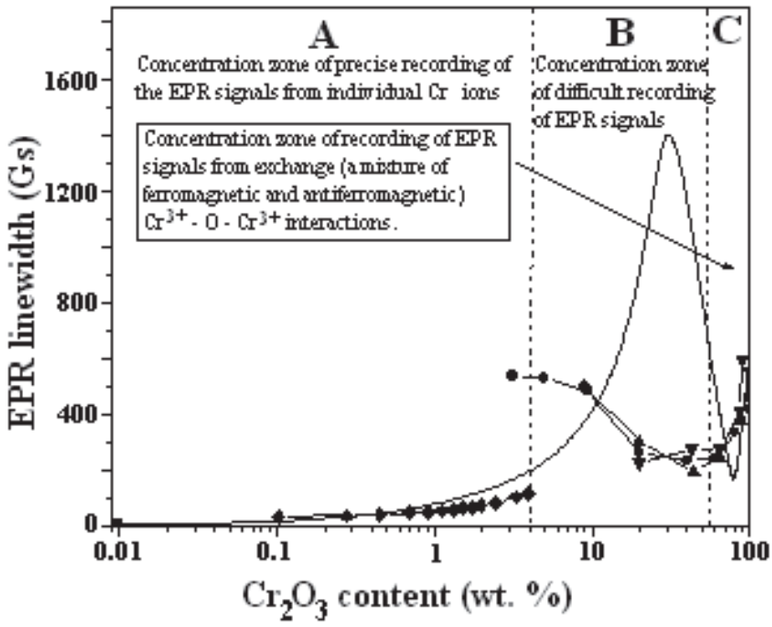

Fig. 11. The dependence of the EPR linewidth on the amount of α-Cr_2O_3 in α-$Cr_xAl_{2-x}O_3$ samples for T = 400 K (100wt % of α-Cr_2O_3 corresponds chromium concentration in the sample of 40 mol %). The solid curves is a dependence of the linewidth for a homogeneous distribution of a chromium impurity in the samples; (●) — experimental data of (Stone & Vickerman 1971); (◆) data of (de Biasi & Rodrigues 1985); (▼) data of (Wertz & Bolton 1972); (▲) data of (Kittel & Abrahams, 1953); (■) data of (Berger et al., 1995). A is the concentration zone of precise recording of the EPR signals from individual Cr^{3+} ions; B is the concentration zone of difficult recording of EPR signals; C is the concentration zone of recording of EPR signals from exchange (a mixture of ferromagnetic and antiferromagnetic) Cr^{3+} - O - Cr^{3+} interactions.

3.3.3 Diffusion processes in α-Al_2O_3 + $n\alpha$-Cr_2O_3 during laser treatment

The process of dissolution of the α-Cr_2O_3 particles in the Al_2O_3 melt is diffusion of surface chromium atoms in the volume of the melt. As result, the chromium diffusion profile (i.e., a smooth curve of the concentration *c* vs. distance, *r*) around undissolved α-Cr_2O_3 particles are formed

$$C_x = C_0 erfc \frac{r}{2\sqrt{Dt}} \quad (4)$$

where D is the diffusion coefficient, t is the heat treatment time (Akulova, 1986). From this expression it follows that the impurities are inhomogeneously distributed in the sample. Thus, each registered EPR spectrum of such a sample is a superposition of signals from Cr^{3+} ions located in different concentration states of the sample (from 0 to 100 wt % of Cr_2O_3). From this standpoint, the manifestation of one or another features of the spectra (e.g., the presence or the absence of singularities I—IV and a signal *A*) reflects a certain statistics of the Cr^{3+} concentration distribution in the sample. To determine the statistics, not only individual singularities, but the whole spectrum must be processed. Note that in the formation of narrow singularities, the zones of the sample with a low local content of the impurity play the main role. The zones with $c \leq 1.0$ mol % play particular role in this respect. In the case when diffusion profiles of the nearest α-Cr_2O_3 particles are not overlapped, the shape of the spectra is independent of their amount (n) in the samples, and the spectrum intensity is proportional to n.

A change in the shape of the EPR spectrum with increasing n (Fig. 8) indicates the overlapping of the chromium diffusion zones of the nearest α-Cr_2O_3 particles. In Fig. 12, a scheme of overlapping of the diffusion profiles about the nearest α-Cr_2O_3 particles depending on their on the amount (i.e., on the change in the distance l between them) in the samples is shown. From Fig. 12, it is seen that the decrease in l is accompanied by a decreasing in the volume of the low-concentration zones A in the samples. The volume of the high-concentration zones C located near α-Cr_2O_3 particles is nearly proportional to the amount of these particles in the specimen.

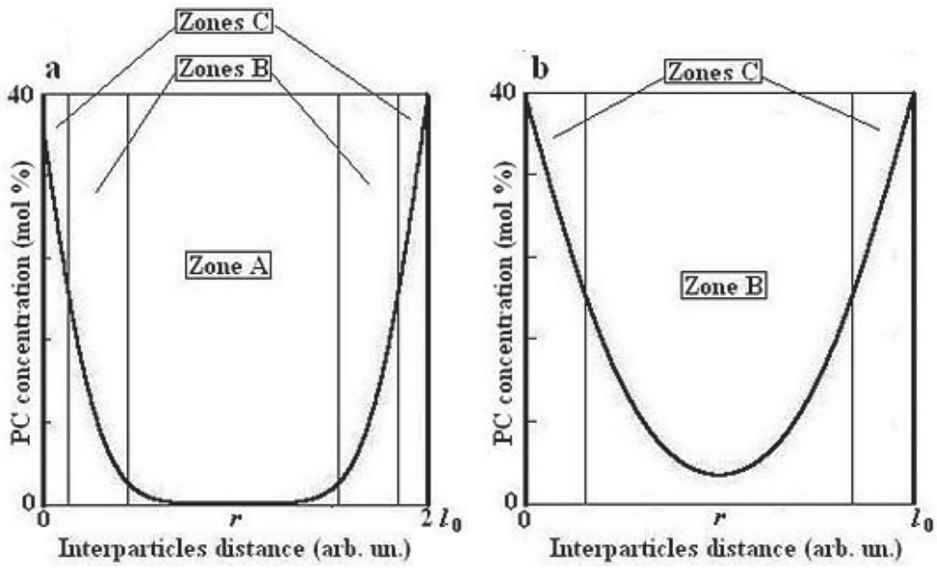

Fig. 12. Scheme of overlapping of concentration diffusion profiles between the nearest α-Cr_2O_3 particles depending on the distance between them: a — the interparticle distance is $2l_0$ (in arb. un.); b — the interparticle distance is l_0 (in arb. un.). A is the concentration zone of precise recording of the EPR signals from individual Cr^{3+} ions; B is the concentration zone of difficult recording of the EPR signals; C is the concentration zone of recording of the EPR signals from exchange (a mixture of ferromagnetic and antiferromagnetic) Cr^{3+} - O - Cr^{3+} interactions.

These analyses explain the nature of changes in the observed EPR spectra. At small values of *n* (insignificant overlapping of diffusion zones), the low-concentration regions (c ~ 0.5 mol %) occupy the maximal volume of the specimen. Though the total content of the impurity in these zones is insignificant, due to small widths of curves, we observe clear intensive singularities, on the background of which a weak and wide signal from high-concentration regions is poorly distinguishable. As *n* increase, the diffusion zones of the nearest particles begin to overlap. It favors a decrease in the volume of low-concentration zone. The amplitudes of singularities I - IV decrease, and the amplitude of the signal A continues to increase proportionally to *n*.

Angular dependences of the amplitudes of singularities II and III (Fig. 10) confirm the textured character of the samples after the laser beam surface treatment (Kakazey et al., 2002). However, relatively small changes in the amplitudes of these signals (for φ = 0 and 90°, they range from ~ 15 % to ~ 20 %) indicate that the Cr^{3+} ions located both in the strongly textured surface layer and in the part of the sample which is not textured take part in the formation of these singularities. This part includes regions of the sample adjacent to the surface layer. The temperature of these regions was lower than the melting point of Al_2O_3, but it was sufficient to cause the local sintering and different types of diffusion processes.

Obtained results show that the melting of the surface layers of pressed α-Al_2O_3 + *n*α-Cr_2O_3 samples take place during the performed laser treatment. In such a layer the Al_2O_3 melt covers the α-Cr_2O_3 particles. The α-Cr_2O_3 particles dissolve gradually in Al_2O_3 with the formation of a number of α-$Cr_xAl_{2-x}O_3$ mutual solid solutions throughout the composition range from x = 0 to x = 2. Complete dissolution of α-Cr_2O_3 in Al_2O_3 does not occur. During cooling of the sample the crystallization of the α-Al_2O_3 layer take place. The crystallized layer show preferred orientation, which is different in different samples. In the surface layer the undissolved α-Cr_2O_3 particles also acquire preferred orientation, the direction of which does not coincide with the direction of the preferred crystallization of α-Al_2O_3. Dissolution of Cr_2O_3 particles in α-Al_2O_3 leads to appearance of the EPR spectra of Cr^{3+} centers in α-Al_2O_3. Analysis of changes of width singularities and the shape of the EPR spectra with an increasing of content of paramagnetic centers shows that the distribution of chromium impurities in α-Al_2O_3 is determined by the diffusion laws. This distribution is inhomogeneous and depends on the amount of α-Cr_2O_3 particles in the samples.

The observed EPR spectra reflect the statistics of the inhomogeneous concentration distribution of the Cr impurity in the samples. To determine the statistics of the concentration distribution of the impurity in the sample on the basis of EPR data, a computer analysis of the whole spectrum, rather than an analysis of individual singularities, must be performed.

3.4 Laser synthesis of crystalline $Al_2O_3:Cr^{3+}$ rods (Vlasova, Kakazey, et al., 2010)

It is necessary to expect that the decreasing of laser beam surface scanning velocity lead to the increasing of the heat energy absorbed by molten layer and the increasing of it width and depth at cross section (Rastogi & Asundi, 2011; Ready, 2001; Shishkovskii, 2009; Weber, 1994). Thus conditions of crystallization of a melt improves. In turn, it supposes the possibility of use of a superficial laser fusion for obtaining crystalline samples from polycrystalline objects (from pressings, ceramics and others).

Cylindrical ceramic specimens were irradiated with an LTN-103 continuous-action Nd^{3+}:YAG facility (Russia) using a wave length λ = 1064 μm. The diameter of the laser spot

was 0.2 mm. The power (P) of irradiation was 70 W. The laser beam was traversed over the surface of the specimens at a traverse rate of a coordinate table (v) of 0.0094, 0.019, and 0.075 mm/s. The irradiation of specimens was performed along their long axes. Specimens were placed in channels formed on surfaces of compacts made from the same mixture by one-pass treatment with a laser beam. After irradiation, the specimens had the shape of rods with a length of 5 to10 mm and a diameter of 1.5 to 2 mm. In Fig. 13, an irradiated specimen removed from a track is shown.

Fig. 13. View of a specimen after laser irradiation at P = 70 W and v = 0.0094 mm/s.

After one-pass laser treatment, on the cross-section of a rod, several zones are distinguished. On the irradiated surface of the specimen, large pores and cracks form. On the opposite side of the specimen, much smaller pores are present. The central part of the rod (in the radial direction from the irradiated surface) is most homogeneous (Fig. 14). In the lower part of the specimen, the formation of necks between particles takes place (see Figs. 15 a, a'), which is characteristic of the process of sintering of powders. In Fig. 15 a, this sintering zone is marked by S. The core (central part) of the specimen consists of polycrystals of different size (Fig. 15 b). More homogeneous zones are dark (see Fig. 15 b, b'). They can be considered monocrystalline regions. In Fig. 15 b', one of such regions is marked by M. On the surface of the specimen, including a part of the lateral surface, fracture along grain boundaries (Fig. 15 c) and reprecipitation of vapor-gas products inside pores (Fig. 15 c') are observed. The rough assessment of the thickness of the melting-recrystallization zone of corundum (h_1) and the thickness of the sintering zone (h_2) shows that h_1 increases substantially as the traverse rate of the laser beam decreases (Fig. 16).

The fracture (cleavage) of the specimens occurs along grain boundaries of ruby (in the sintering zone) and along boundaries of microcrystallites (in the recrystallization zone) (Fig. 17). Crystallites have a lamellar (tabular) shape. The size of crystallites in the lower part of the specimen ranges from ~10 to ~30 μm. In the central part of the specimen, the size of crystallites ranges from ~25 to ~40 μm. In the surface layer, their size increases to about 35–53 μm.

In the initial nonirradiated Al_2O_3–Cr_2O_3 specimens, only a weak broad EPR signal, which was due to defective states of the α-Cr_2O_3 phase, was registered at g ~ 1.9. After laser treatment, EPR signals of both typical isotropic polycrystalline singularities (I—IV at $H_I \approx$ 5337 Gs, $H_{II} \approx$ 4505 Gs, $H_{III} \approx$ 1909 Gs, and $H_{IV} \approx$ 340 Gs) of different intensities and sets of EPR signals with a strong angular dependence were registered (Fig. 18 b).

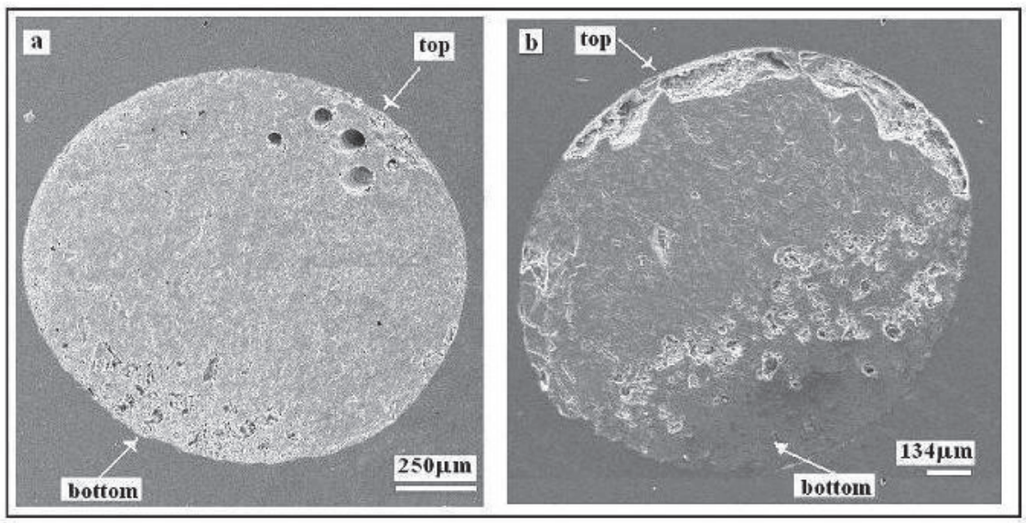

Fig. 14. Micrographs of cross-sections of specimens after laser treatment. P = 70 W. (a) v = 0.0094 mm/s; (b) v = 0.075 mm/s.

Analysis of the EPR spectrum of Cr^{3+} (singularities I—III) in Al_2O_3 polycrystalline samples we have made in part 3.3 (see also (Carman & Kroenke, 1968; de Biasi & Rodrigues 1985; O'Reilly & Maciver, 1962; Stone & Vickerman, 1971). Figures 9 and 18 a shows that singularity I corresponds to the transition -3/2 ↔ -1/2 of ions Cr^{3+} in Al_2O_3 (θ = 90°, where θ is the angle between crystal axes *c* and the direction of the magnetic field). Singularity II corresponds to the transition -1/2 ↔ +1/2 (θ =35°). Singularity III corresponds to the +1/2 ↔ +3/2 transition (θ = 90°). Singularity IV is a forbidden transition (FT) (θ = 0 – 30°).

The observation of the strong angular dependence of the set of EPR signals (Figs. 18 b, 3) implies that, under laser treatment, the formation of several Cr^{3+}:Al_2O_3 monocrystals in samples take place. The width of these lines ranges from ~40 to ~50 Gs. The angular dependences of the EPR signals agree well with the positions of singularities I –IV (see Fig. 18b, 19), which indicates that anisotropic EPR signals correspond to Al_2O_3:Cr^{3+} crystals oriented differently in the specimen.

In general, the angular dependence of the EPR spectrum of the crystal is dependent on the crystal orientation. In Fig. 18a, such a dependence for the case where the crystal axis *c* is perpendicular to axis of rotation (ψ = 90° and angle θ are between 0 and 180°) is shown. In the case where ψ ≠ 90°, during crystal rotation in the magnetic field, the angle θ is larger than 90° – ψ and smaller than 90° + ψ. The character of the angular dependence of the EPR spectrum of Cr^{3+} in Al_2O_3 for ψ = 75°, ψ = 60° and ψ = 45° are shown in Fig. 20.

From the performed analysis it follows that, independently of the orientation of crystalline formations in the specimen, the angular dependences of all EPR lines of the fine structure pass through the central part of the spectrum ($H_{III} < H < H_{II}$). Note that, in this part of the spectrum, the superposition of the EPR lines of different formations (crystals) complicates their rigorous identification. In the region $H_{IV} < H < H_{III}$, the transitions-3/2 ↔-1/2, +1/2 ↔ +3/2 (θ =90°) and a forbidden transition (FT) show an angular dependence. In the region $H > H_I$, only the transitions +1/2 ↔ +3/2 show an angular dependence. Thus, the lines of the last transitions can serve as a probe of the number of monocrystalline formations and their approximate orientation in the sample.

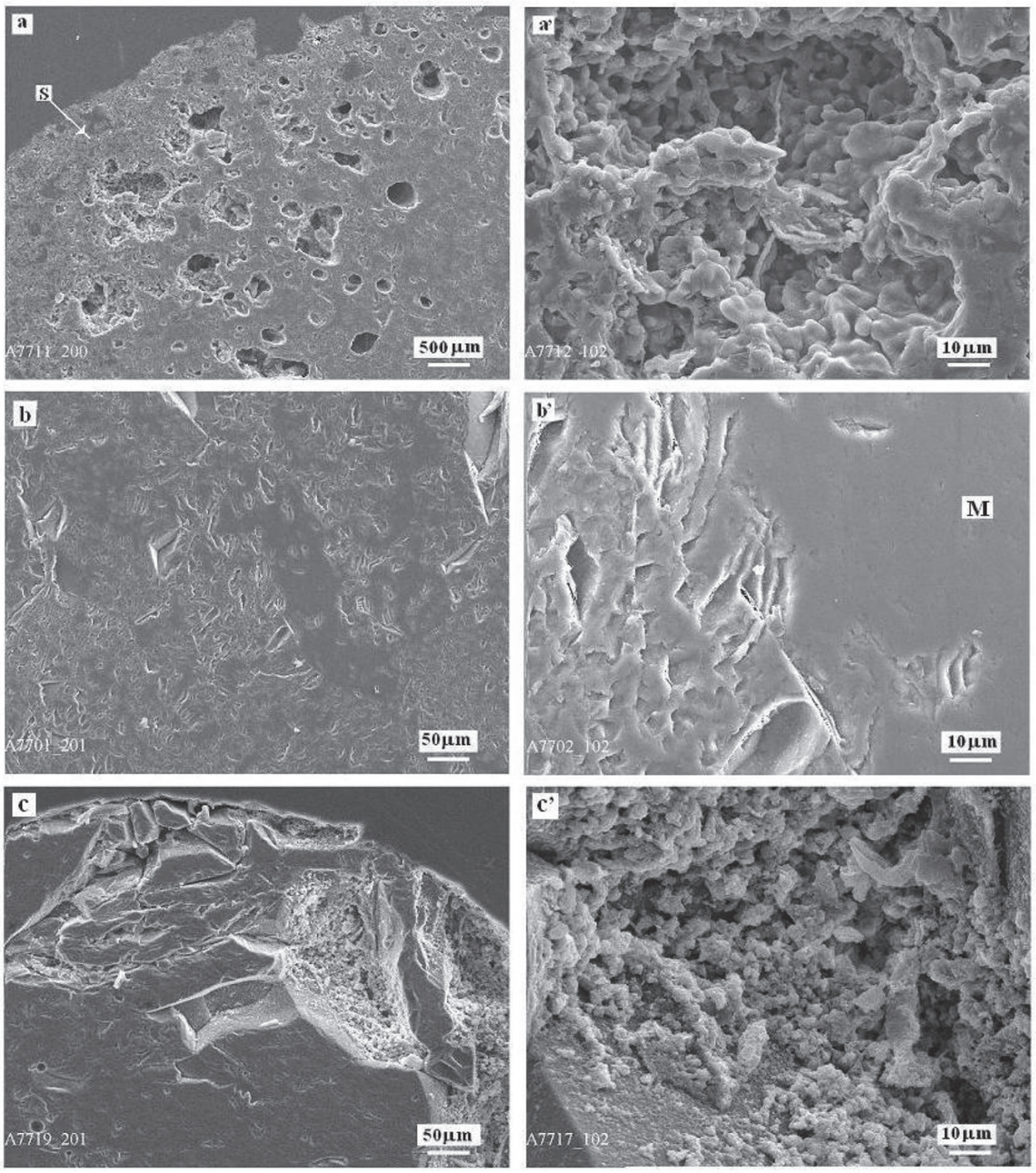

Fig. 15. Micrographs of cross-sections of specimens after laser treatment at P = 70 W and v = 0.075 mm/s. (a, a′) the lower surface of the rod ; (b, b′) the middle part of rod; (c, c′) the upper surface of the rod. S designates the sintering zone and M designates the monocrystalline zone.

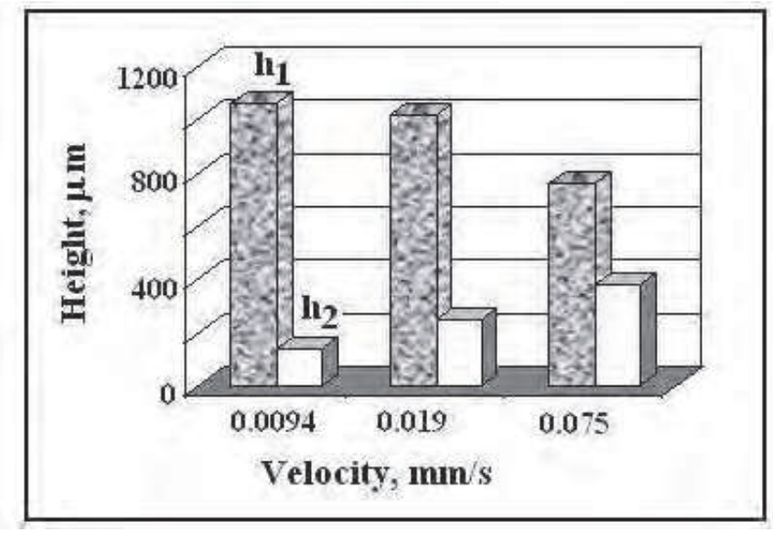

Fig. 16. Changes in the maximal values of the thickness of recrystallized layer (h_1) and the thickness of the sintered layer (h_2) depending on the traverse speed of the laser beam. P = 70 W.

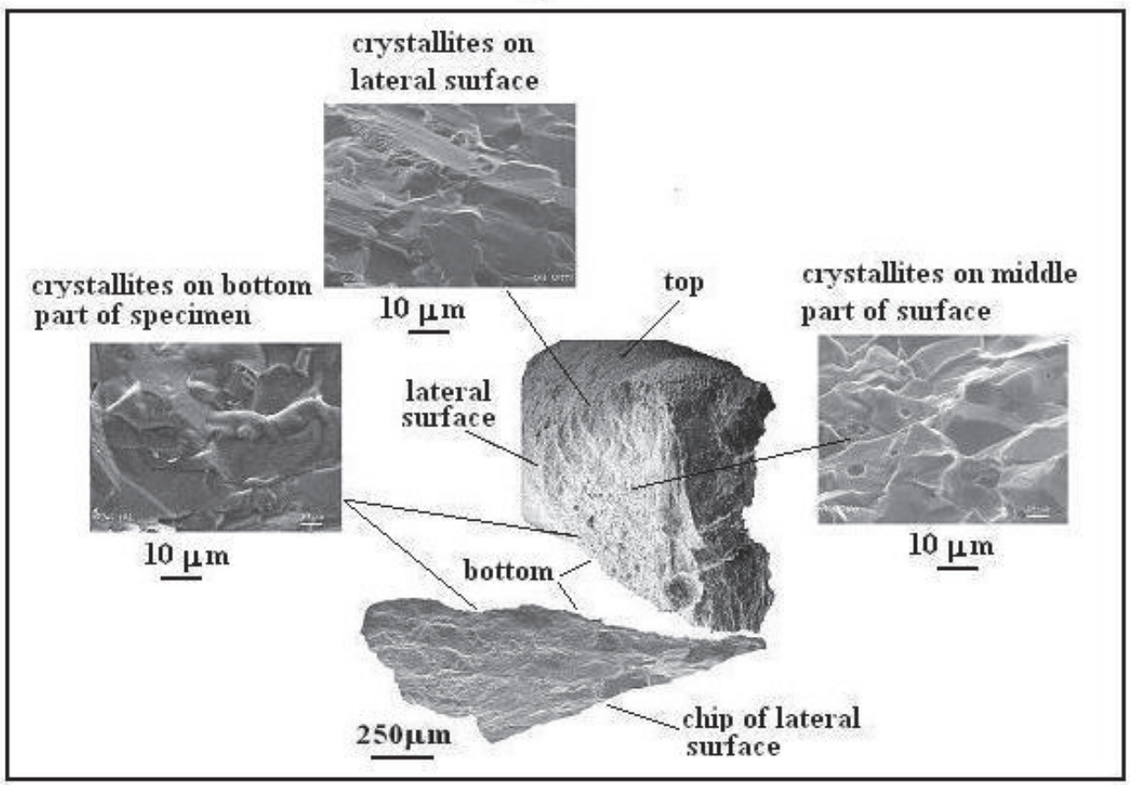

Fig. 17. Micrographs of a chip of a specimen after laser treatment at P = 70 W and v = 0.075 mm/s.

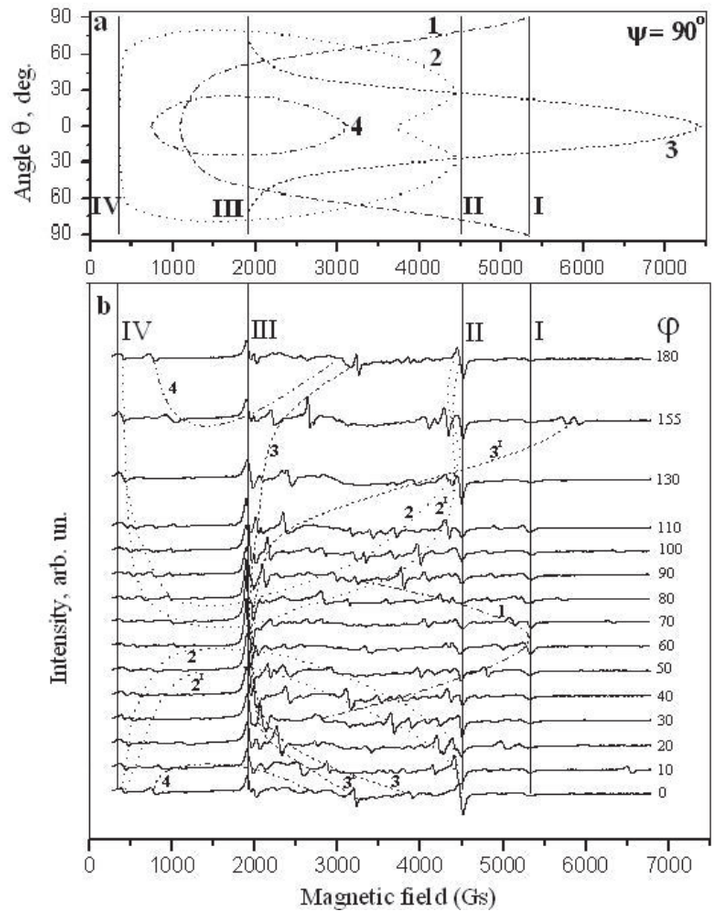

Fig. 18. Angular dependences of the EPR spectrum of Cr^{3+}:Al_2O_3 in: a) monocrystal, ψ = 90°; b) laser-synthesized rod. The axis of rod was inclined at an angle of 90° to the axis of rotation. 1, 1' corresponds to the -3/2 ↔ -1/2 transition; 2, 2' corresponds to the -1/2 ↔ +1/2 transition; 3, 3' corresponds to the +1/2 ↔ +3/2 transition; 4, 4' correspond to the forbidden transition; I, II, II, and IV are singularities of transitions 1, 2, 3, and 4, respectively, in the polycrystalline part of the specimen. Signals 1, 2, 3 and 4 and 1 ', 2 ', 3 ' and 4 ' correspond to large crystallites of different orientations in the rod.

The performed analysis of the angular dependences (Figs. 18b, 19) shows that about 7 monocrystalline formations of nearly equal sizes (~0.3 mm) are present in the investigated specimen. These monocrystals have an arbitrary orientation. None of the axes of crystals coincides with the direction of the axis of synthesis of the rod. At the same time, the intensities of singularities I – IV show anisotropy, which is typical of textured polycrystalline specimens. Unfortunately, by virtue of the fact that these signals are overlapped with the signals from monocrystalline formations, precise measurements of angular amplitude changes are complicated. According to our rough assessments, the plane of texturing of the polycrystalline part of the specimen is inclined by an angle of ~20 to ~30° to the axis of the investigated rod.

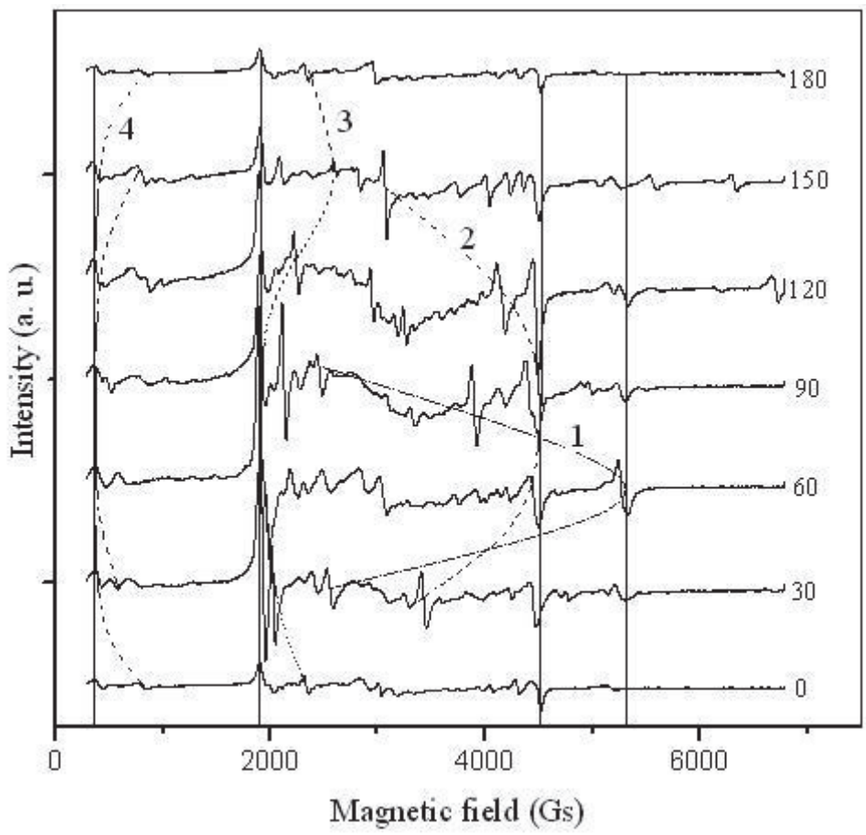

Fig. 19. Angular dependence of the EPR spectrum of Cr^{3+} in a laser-synthesized rod. The axis of rod coincides with axis of rotation. Others symbols are as in Fig. 18.

Thus, the results obtained by the EPR method show that, during the laser treatment of α-Al_2O_3–Cr_2O_3 rods, a number of processes are realized. These are: the formation of the solid solution Al_2O_3:Cr_2O_3 (the synthesis of ruby), the formation of textured polycrystalline regions in the specimen (the plane of texturing is inclined by an angle of about 20–30° to the axis of the rod), and the formation of ruby monocrystals in the rod. The direction of the axes *c* of these crystals is arbitrary.

The performed investigations showed that, in the chosen irradiation mode of the 97 wt. % Al_2O_3 + 3 wt. % Cr_2O_3 mixture, polycrystalline ruby with monocrystalline inclusions of different size was synthesized. This means that, in the narrow irradiation zone, synthesis of ruby, which includes the penetration of Cr^{3+} ions into the corundum lattice, is realized. In this context, we can speak about selective laser synthesis of ruby.

The polycrystalline part consists of differently directed crystallites, which are predominantly concentrated in the sintering zone and partially in the melting zone. Monocrystals form in the melting zone of corundum. Since the growth conditions of monocrystals depend on thermophysical processes (on the ramification of the heat flow in the vertical and horizontal direction) (Bagdasarov, 2004; Bagdasarov & Goryainov, 2001; Bagdasarov & Goryainov, 2007; Lukanina et al., 2006), in the melting-recrystallization zone, the size of crystallites increases as the distance from the irradiated surface decreases.

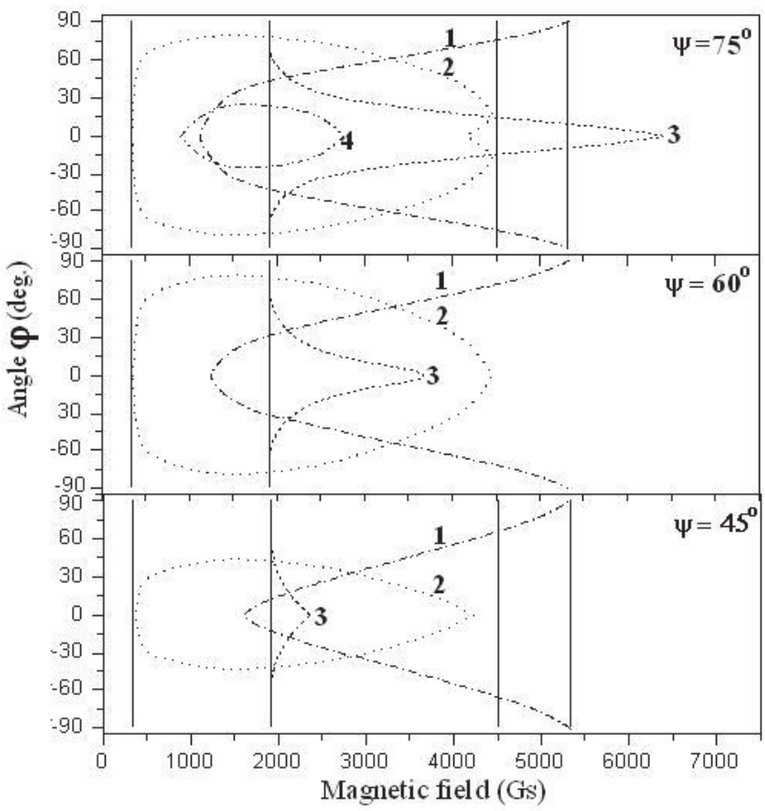

Fig. 20. Angular dependences of EPR spectrum of Cr^{3+} in a crystalline Al_2O_3 specimen for different values of ψ.

As in the case of HDC of ruby monocrystals, for horizontally directed laser synthesis of ruby, there exists a strong dependence of the sizes of the melting-recrystallization zone and sintering zone on the traverse rate of the beam at the chosen power of beam. This is due to the distribution of temperature from the surface to the bulk of the specimen (a temperature gradient). From Fig. 16 it follows that the traverse rate of the beam must be much less than 0.0094 mm/s. Judging from traditional HDS of corundum monocrystals (Bagdasarov & Goryainov, 2001; Lukanina et al., 2006), v must approach the value of about 0.0027 to 0.0022 mm/s.

The presence of a large number of pores of various size in the lower part of the rod (see Figs. 14, 15a, a ') is caused by a number of factors, namely, the incompleteness of the sintering process and shrinkage (Vedula et al., 2001) and the absence of the sufficient amount of a corundum melt. With increase in the amount of the melt, the porosity substantially decreases (see Figs. 14, 15b, b'). However a part of intergranular voids are encapsulated. Under complete melting of the material, these microvoids cause the blistering of the melt and remain in the volume of the material during its crystallization (Dobrovinskaya et al., 2009; Malukov et al., 2008). The formation of large pores and damages in the upper part of the rod (on an irradiation surface) is predominantly caused by the development of high-temperature processes of dissociation of Al_2O_3 (Ristic et al., 2009; Pankratz, 1982). The reprecipitation of vaporous products in pores (see Fig. 15 c, c ") is a confirmation of the given assumption. Nucleation of cracks in the volume and on the lateral surfaces of the rod

(see Figs. 15c, 17) is a direct consequence of the development of thermal stresses and the plastic deformation, which arise as the front of crystallization moves (Denisov et al., 2007; Ivanovic et al., 2003; Lebedev et al., 2008; Samsonov, 1973).
Note that the commonly used sintering temperature of corundum powders ranges from 1700 to 1750°C (Ivanovic et al., 2003). The melting point and sublimation point of Al_2O_3 are 2046 and 2980°C, respectively (Pankratz, 1982 ; Samsonov, 1973). Consequently, on the irradiated surface, a temperature of about 3000°C develops, and the average temperatures in the melting-recrystallization zone and in the sintering zone are about 2000 and 1700°C. In each zone, temperature decreases with distance from the irradiated surface.

4. Conclusion

Depending on intensity of an irradiation and velocity of removing of a laser beam on a surface of pressings from powder mixtures Al_2O_3:Cr_2O_3 a number of physical and chemical processes is passing (Weber, 1994 proceeds; Ready, 2001; Rastogi and Asundi, 2011; Shishkovskii, 2009)., defined by non-uniform character of distribution of temperature on volume of the sample. In a superficial layer the temperature reaches the maximum value ~ 3000 °C. This initiates not only evaporation of material but also its dissociation. As a result, in a superficial zone of specimens a layer of Al_2O_3 with high deficiency is formed. This layer has a raised electrocoductivity. In a fusion zone dissolution Cr_2O_3 in Al_2O_3, formation of solid solution Cr^{3+} : Al_2O_3 takes place. The new result is that during process of cooling-crystallization in this layer a textured packing from crystalline particles is forming. This is typical for all processed surfaces. The direction of texturing has casual character. Most likely, texturing is set by crystallization conditions in an irradiation starting point. Supervision in some samples of several directions of texturing is connected with heterogeneity of packing of particles in pressings. The sintering zone is set by temperature range: T_{melt} ÷ ~2/3 T_{melt}. Owing to it it isn't homogeneous neither on structure, nor on properties. In this zone formation of non-uniform solid solution Cr^{3+}: Al_2O_3 is observed. In layers close to a fusion zone more dense packing of particles of a powder, than in the layers adjoining to non-sintered part of pressings is marked.
Decreasing of velocity of scanning of a laser beam on a surface of polycrystalline specimen leads to an increase of sizes of zone of a heating-melting. This allows to spend out a laser fusion in region 10 times more the size of a spot of an irradiation. After treatment in such regime of Al_2O_3-Cr_2O_3 specimens the formation of several large crystallites of a ruby was observed. These results show possibility of laser synthesis of crystals of a ruby with the considerable big sizes.

5. Acknowledgment

The authors wish to thank CONACYT for financial support (Project 48361).

6. References

Akulova, L. T.; Vlasova, M. V.; & Kakazey, M. G. (1986). Interaction of melt glass with chromium diboride, *Glass Phys. Chem*., Vol.12, No. 5, pp. 574-578
Ali, J.; Bennett W. & Herriot, D. (1960) (US Patent 3,149,290)

Bagdasarov, H. S. (2004). *The High Temperature crystallization from melt*, Moscow, Pub. Phismatlit, 160, (in Russia)

Bagdasarov, H. S. & Goryainov, L. A. (2007). *Heat and mass transfer at a growing of monocrystals by directed crystallisation*, Moscow, Pub. Phismatlit, 224, (in Russia)

Bagdasarov, H. S. & Goryainov, L. A. (2001). Thermal processes of a growing of monocrystals of sapphire by the horizontal directed crystallisation, *Perspective materials*, No.6, pp. 45-50, (in Russia)

Bai, P. & Li, Y. (2009). Study on high temperature sintering processes of selective laser sintered Al_2O_3/ZrO_2/TiC ceramics, *Science of Sintering*, Vol. 41, No.1, pp. 35-41

Barnes, S. E. (1974). Fine-structure splitting of a localized moment in a metal: A diagrammatic analysis, *Phys. Rev. B*, Vol..9, pp. 4789 - 4807

Berger, R.; Kliava, J.; Yahiaoui, E.; Bissey, J.-C.; Zinsou, P.K. & Beziade, P. (1995). Diluted & non-diluted ferric ions in borate glasses studied by electron paramagnetic resonance, *J. Non-Cr. Sol*., 180 [2] 151-163

Carman, C. J. & Kroenke, W. J. (1968). Electron spin resonance of α-chromia-alumina solid solutions, *J. Phys. Chem*., Vol.12, pp. 2562-2566

Da Shen, L.; Huang, Y.H.; Tian, Z. J. & Hua, G. R. (2007). Direct Fabrication of Bulk Nanostructured Ceramic from Nano-Al_2O_3 Powders by Selective Laser Sintering, *Key Engineering Materials*, v. 329 (Advances in Abrasive Technology IX), pp. 613-618

De Biasi, R.S. & Rodrigues, D.C.S. (1985). Measurement of small concentrations of Cr & Fe in α-Al_2O_3 using electron spin resonance, *J. Am. Ceram. Soc*., Vol.68, No.7, pp. 409-412

Deckard, C. R. (1988). *Selective laser sintering*, University of Texas at Austin

Denisov, A. V.; Ktumov, V. M. & Punin, Yu. O. (2007). Investigation of optical anomalies & residual stress in base facetting tapes of sapphire crystals grown up by a method of Stepanov, *Phys. Solid State*, Vol. 49, Iss. 3, pp. 454-459

Dobrovinskaya, E. R.; Lytvinov, L. A. & Pischik, V. (2009). *Sapphire. Material, Manufacturing, Application*, New York, Springer, 481

Dorre, E. & Hubner, H. (1984). *Alumina Processing, Properties, & Applications*, Springer-Verlag, New York

Ferkel, H.; Naser, J. & Riehemann, W. (1997). Laser-induced solid solution of the binary nanoparticle system Al_2O_3-ZrO_2, *Nanostructured Materials*, Vol. 8, No. 4, pp. 457-464

Gahler, A.; Heinrich, J. & Gunst, G. (2009). Direct laser sintering of Al_2O_3-SiO_2 dental ceramic components by layer-wise slurry deposition, *J. American Ceramic Society*,Vol. 89, No.10, pp. 3076-3082

Galoisy, L. & Calas, G. (1993). Inhomogeneous distribution of Cr impurities in α –Al_2O_3 during refractory aging," J. Mater. Res., Vol.8, No. 5, pp.1153 -1157

Gebhardt, A. & Hancer, C. (2003). *Rapid prototyping*, Verlag, Munich

Goodison, P., (2008). RYA *Laser Handbook*, Royal Yachting Association

Hurle, D.T. J. (1994). *Handbook of crystal Growth., v. 2a, Basic Techniques*, North-Holl&, Amsterdam

Injeyan, H. & Goodno, G. (2011). *High Power Laser Handbook*, McGraw-Hill Higher Education

Ivanovic, M. R.; Nenezic, M. & Jokanovic, V. (2003). High Temperature Sintering Kinetics of α-Al_2O_3 Powder, Sci. Sintering, Vol. 35, pp. 99-102

JCPDS-International Centre for Diffraction Data (1999).

Kakazey, M.; Vlasova, M.; Gonzalez-Rodriguez, J.G. & Salazar-Hernández, B. (2002). Fine structure of EPR spectra of Fe^{3+} in α-Al_2O_3 crystal, powders, & textured ceramics, *Mat. Sci. Eng. B*, Vol.90, No. 1-2, pp. 114-119

Kakazey, M.; Vlasova, M.; Márquez Aguilar, P. A.; Bykov, A.; Stetsenko, V. & Ragulya, A. (2009). Laser Surface Solutionizing & Crystallization of Al_2O_3-Cr_2O_3, *International Journal of Applied Ceramic Technology*, Vol. 6, No 2, pp. 335-343

Kittel, C. & Abrahams, E. (1953). Dipolar Broadening of Magnetic Resonance Lines in Magnetically Diluted Crystals, *Phys. Rev.*, Vol.90, No. 2, pp.238-239

Kliava, J. (1988). EPR Spectroscopy of Disordered Solids, Zinatne, Riga

Knappwost, A. & Gunsser, W. (1959). Magnetic resonance absorption in mixed crystal a-Al_2O_3-Cr_2O_3 by aid of a modified reflection method, *Z. Phys. Chem. N.F.*, Vol. 21, pp.305-325

Lebedev, G. A.; Malukov, S. P.; Stefanovich, V. A. & Cherednichenko, D. I. (2008). Thermophysical processes during sapphire crystal growth by the horizontal Bridgman method, Crystallography Reports, Vol. 53, No. 2, pp. 331-335

Liu, Z. H.; Nolte, J. J.; Packard, J. I.; Hilmas, G.; Dogan, F. & Leu, M. C. (2007). *Selective Laser Sintering of High-density Alumina Ceramic* Parts, Proceedings of the 35th International MATADOR Conference, Springer, London, pp. 351-354

Lukanina, M. A.; Hodosevitch, K. V. ; Kalaev, V. V.; Semenov, V. B.; Sytin, V. N. & Raevsky, V. L. (2006). 3D numerical simulation of heat transfer during horizontal direct crystallization of corundum single crystals, *J. Crystal Growth*, v.287, Iss. 2, pp. 330-334

Lyubo, B. Ya. (1975). *The crystallisation theory in large volumes*, Moscow, Nauka (in Russia)

Maiman, T. H. (1960). Stimulated optical radiation in ruby. *Nature,* Vol. 187, No.4736, pp. 493–494

Majumdar, J. D.; Chandra, B. R.; Mordike, B. L.; Galun, R. & Manna, I. (2004). Laser surface engineering of a magnesium alloy with Al+Al_2O_3, *Surf. Coat. Technol.*, Vol.179, No. 2-3, pp. 297-305

Malukov, S. P.; Stefanovich, V. A. & Cherednichenko D. I. (2008). Study of model of self-coordinated growth of single crystals of sapphire by horizontal directed crystallization, *Semiconductors*, Vol. 42, No.13, pp.1508-1511

Manenkov, A. A. & Prokhorov, A. M. (1955). The fine structure of the paramagnetic resonance of the ion Cr^{3+} in chromium corundum, *Soviet Phys.-JETP*, Vol.1, pp.611-616

McGuire, T. R.; Scott, E. S. & Grannis, F. H. (1956). Antiferromagnetism in a Cr_2O_3 Crystal, *Phys. Rev.*, Vol.102, No. 4, pp. 1000-1003

Nubling, R. K. & Harrington, J. (1997). Optical properties of single-crystal sapphire Fibers, *Applied Optics*, Vol.36, No. 24, pp.5934-5940

O'Reilly, D. E. & Maciver, D. S. (1962). Electron paramagnetic resonance absorption of chromia-alumina catalysts, *J. Phys. Chem.*, Vol. 6, pp. 276 – 281

Pampuch, R. & Haberko, K. F. (1997). *Role of Ceramics in a Self-Sustaining Environment,*: "Techna".

Pankratz, L.B. (1982). Thermodynamic properties of elements & oxides, U.S. Bur. of Mines., No. 672. p. 509

Poole, C. P. & Itzel, J. F. (1964). Electron Spin Resonance Study of the Antiferromagnetism of Chromia Alumina, *J. Chem. Phys.*, Vol. 41, No. 2, 287-295

Quispe Cancapa, J. J.; De Arellano Lopez, A. & Saoir, R., A. (2002). Propiedades Mecanicas de Fibras de Al_2O_3 Dopadas con Cr_2O_3 Fabricadas por Fusion Laser, VIII Congreso Nacional de Propiedades Mecanicas de Solidos, G&ia, pp.691-697

Rastogi, P. & Asundi, A. (2011). Optics and Lasers in Engineering,

Ready, J.F. (1971). *Effects of high-power laser radiation*, Academic Press, New York-London

Ready, J. F (2001). *LIA Handbook of Laser Materials Processing*, Published by the *Laser* Institute of America

Ristic, M.; Vlasova, M.; Ragulya, A.; Stetsenko, V.; Kakazey, M.; Márquez Aguilar, P.A.; Timofeeva, I. ; Tomila, T. & Juarez Arellano, E. A. (2009). The layer by layer selective laser sintesis of ruby, *Report on "International Conference Sintering*, Kiev, Ukraine, 7-11 september, 2009

Samsonov, G. V. (1973). *The Oxide handbook*. New York, IFI/Plenum, 524 Maiman, T. H. (1960). Stimulated optical radiation in ruby. *Nature,* Vol. 187, No.4736, pp. 493–494

Shevchenko, V. Ya. & Barinov, S. M. (1993). *Engineering Ceramics* [in Russian], "Nauka", Mosco

Shishkovskii, I. B. (2005). Selective Laser Sintering and Synthesis of Functional Structures [in Russian], Author's Abstract of the Doctor's Degree Thesis (Physico-Mathemathical Sciences), Chernogolovka

Shishkovskii, I. V. (2009). *Laser Synthesis of Functional Mesostructures and Bulk Articles* [in Russian], "Fizmatlit", Moscow

Shishkovsky, I.; Yadroitsev, I.; Bertrand, Ph. & Smurov, I. (2007). Alumina–zirconium ceramics synthesis by selective laser sintering/melting, *Applied Surface Science*, Vol. 254, No.4, pp. 966-976

Statz, H. ; Rimai, L. ; Weber, M. J. ; de Mars, G. A. & Koster, G. F. (1961). Chromium Ion Pair Interactions in the Paramagnetic Resonance Spectrum of Ruby*, J. Appl. Phys*., Vol. 32, pp. 218S-220S

Stone, F. S. & Vickerman, J. C. (1971). Magnetic properties of chromium ions in oxide matrices. 1. Solid solution, *Trans. Faraday Soc*., Vol. 67, pp. 316 – 328

Subramanian, P. K. & Marcus, H. L. (1995). *Selective Laser Sintering of Alumina Using Aluminum Binder*, Materials and Manufacturing Processes, Vol. 10, Iss. 4, pp. 689 – 706

Subramanian, P. K. ; Zong, G. ; Vail, N. ; Barlow, J. W. & Marcus, H. L. (1993). Selective Laser Sintering of Al_2O_3, *Solid Freeform Fabrication Proceedings,* pp.350-359

Townes, C. H. (1960). *The first laser*. University of Chicago. Retrieved 2008-05-15

Träger, F. (2007). *Handbook of Lasers and Optics*, (Ed.), Springer, XXVI, 1332

Tretyakov, Yu. D. (1987). Ceramics – Material of Future [in Russian], "Znanie", Moscow

Triantafyllidis, D.; Li, L. & Stott, F. H. (2002). Surface treatment of alumina-based ceramics using combined laser sources, *Appl. Surf. Sci.,* Vol.186, No. 1-4, pp.140-144

Triantafyllidis, D.; Li, L. & Stott, F. H. (2004). Laser cladding of high performance ceramic sheets on a low quality ceramic substrate, *Thin Solid Films*, Vol. 453-454, No. 1, pp.80-83

Vedula, V. R.; Glass, S. J.; Saylor, D. M.; Rohrer, G. S.; Carter, W. C.; Langer, S. A. & Fuller, Jr. E. R. (2001). Residual-stress Predictions in Polycrystalline Alumina, *J. Am.Ceram.Soc*., Vol. 84, No.12, pp. 2947-2954

Vlasova, M.; Kakazey, M.; Márquez Aguilar, P. A.; Guardian Tapia, R.; Juarez Arellano, E.; Stetsenko, V.; Ragulya, A.; Bykov, A. & Timofeeva, I. Peculiarites of Ruby

Synthesized from Al_2O_3-Cr_2O_3 Powder Mixture by Selective laser Sintering, *J. Laser Micro/Nano Engineering*, (in press. accept.).

Vlasova, A. G.; Florinskaya, V. A.; Venediktov, A. A.; Dutova, K. P.; Morozov, V. N. & Smirnova, E. V. (1972). *Infrared Spectra of Inorganic Glasses & Crystals*, Edited by A. G. Vlasova, V. A. Florinskaya [in Russian], "Izdatelstvo Khimiya", Leningrad

Vlasova, M.; Ragulya, A.; Stetsenko, V.; Kakazey, M.; Márquez Aguilar, P. A.; Timofeeva, I.; Tomila, T. & Juarez Arellano, E. A. (2010). The Layer by Layer Selective Laser Synthesis of Ruby, *Science of Sintering*, Vol.42, No 1, pp. 3 – 13

Vlasova, M.; Kakazey, M.; Márquez Aguilar, P. A.; Stetsenko, V.& Ragulya, A. (2010). Laser horizontally directed synthesis of ruby, *Superficies y Vacio,* Vol. 23(S), pp.15-20

Wang, H.; Wang, W. Y.; Xie, C. S.; Song, W. L. & Zeng, D. W. (2004). Microstructural characteristics of Al_2O_3-based refractory containing ZrO_2 induced by CO_2 laser melting, *Appl. Surf. Sci.*, Vol. 221, No.1-4, pp. 293-301

Weber, M. J , (2001). *Handbook of Lasers*, CRC Press

Webb, C.E. & Jones, J.D.C. (2003). *Handbook of Laser Technology and Applications* (Three-Volume Set) (Vols 1-3), Taylor & Francis

Weber, M. J (1994). *CRC Handbook of Laser Science and Technology* Supplement 2: Optical Materials (Laser and Optical Science and Technology)

Wefers, K. & Misra, C., (1987). *Oxides & Hydroxides of Aluminum*, Aluminum Company of America

Wenzel, R. F. & Kim, Y.W. (1965). Linewidth of the Electron Paramagnetic Resonance of $(Al_2O_3)_{1-x}(Cr_2O_3)_x$, *Phys. Rev.*, Vol.140, No. 5A, pp. A1592-A1598

Wertz, J.E. & Bolton, J.R. (1972). Electron Spin Resonance. *Elementary theory & Practical application,* McGraw-Hill Book Company, New York,

Xu, Z. ; Zhang, J. ; Zheng, H. ; Cai, C. & Huang, Y. (2005). *Morphology & mechanical properties of PS/Al_2O_3 Nanocomposites Based on Selective Laser Sintering*, J. Mater. Sci. Technol., Vol. 21, No. 6, pp. 866-870

Yen, W. M., (1999). Synthesis, Characterization & Applications of Shaped Single Crystals, *Solid State Phys.*, Vol.41, No.5, pp.770-773

Zum, G. K. -H.; Bogdanow, Ch. & Schneider, J. (1995). Friction & wear reduction of Al_2O_3 ceramics by laser-induced surface alloying, *Wear*, Vol. 181-183, No. 1, pp. 118-128

Zhao, J.-F.; Huang, Y-H.; Hua, G-R.; Zhang, J-H.; Wang, L.; Zhang, Y-K.; Zhou, J-Z. & Zhou, M. (2003). Free fabrication of nano-Al_2O_3 bulk materials by SLS, *Cailiao Kexue yu Gongcheng (Materials Science & Engineering)* (China). Vol. 21, May-June 2003, pp. 339-341

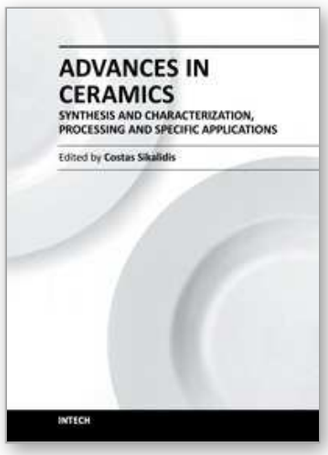

Advances in Ceramics - Synthesis and Characterization, Processing and Specific Applications

Edited by Prof. Costas Sikalidis

ISBN 978-953-307-505-1
Hard cover, 520 pages
Publisher InTech
Published online 09, August, 2011
Published in print edition August, 2011

The current book contains twenty-two chapters and is divided into three sections. Section I consists of nine chapters which discuss synthesis through innovative as well as modified conventional techniques of certain advanced ceramics (e.g. target materials, high strength porous ceramics, optical and thermo-luminescent ceramics, ceramic powders and fibers) and their characterization using a combination of well known and advanced techniques. Section II is also composed of nine chapters, which are dealing with the aqueous processing of nitride ceramics, the shape and size optimization of ceramic components through design methodologies and manufacturing technologies, the sinterability and properties of ZnNb oxide ceramics, the grinding optimization, the redox behaviour of ceria based and related materials, the alloy reinforcement by ceramic particles addition, the sintering study through dihedral surface angle using AFM and the surface modification and properties induced by a laser beam in pressings of ceramic powders. Section III includes four chapters which are dealing with the deposition of ceramic powders for oxide fuel cells preparation, the perovskite type ceramics for solid fuel cells, the ceramics for laser applications and fabrication and the characterization and modeling of protonic ceramics.

InTech Europe
University Campus STeP Ri
Slavka Krautzeka 83/A
51000 Rijeka, Croatia
Phone: +385 (51) 770 447
Fax: +385 (51) 686 166
www.intechopen.com

InTech China
Unit 405, Office Block, Hotel Equatorial Shanghai
No.65, Yan An Road (West), Shanghai, 200040, China
中国上海市延安西路65号上海国际贵都大饭店办公楼405单元
Phone: +86-21-62489820
Fax: +86-21-62489821

IntechOpen